Mannose Transporter of *Escherichia coli.* Backbone Assignments and Secondary Structure of the IIA Domain of the $IIAB^{Man}$ Subunit†

Stephan Seip,‡,§ Jochen Balbach,§ Stefan Behrens,§ Horst Kessler,*,§ Karin Flükiger,‖ Rita de Meyer,⊥ and Bernhard Erni‖,⊥

Institut für Organische Chemie und Biochemie, Technische Universität München, Lichtenbergstrasse 4, 85747 Garching, FRG, Institut fur Biochemie, Universität Bern, Freiestrasse 3, CH-3012 Bern, Switzerland, and Phillips Universität, FB Biologie, Karl von Frisch Strasse, 35043 Marburg, FRG

Received October 19, 1993; Revised Manuscript Received February 9, 1994®

ABSTRACT: The mannose transporter of *Escherichia coli* consists of two transmembrane and one peripheral protein subunit. The complex acts by a mechanism which couples translocation of the substrate with substrate phosphorylation. The peripheral $IIAB^{Man}$ is a homodimer. The $IIAB^{Man}$ monomer itself contains two domains which are linked by an Ala-Pro-rich hinge and which are both transiently phosphorylated at histidyl residues. The IIA and IIB domains can be separated by limited proteolysis. The IIA domain has a dimer molecular mass of 2 × 14 kDa. Almost complete ^{1}H, ^{13}C, and ^{15}N NMR assignments of the backbone resonances of IIA^{Man} have been achieved using 3D and 4D double- and triple-resonance techniques. Secondary structure elements were derived from NOE data. The IIA domain consists of a central β-sheet of four parallel and one antiparallel strand (strand order 5 4 3 1 2) with helices on both sides of the sheet. The active-site His-10 is located in a loop at the C-terminus of β-strand 1. This loop and the loop after strand 3 are at the topological switch point of the sheet.

Solute transport across a biological membrane and against a concentration gradient is an energy-requiring process. The driving force is provided by transmembrane ion gradients, a transmembrane potential difference, the free energy of ATP hydrolysis, or group translocation. The hallmark of group translocation is the coupling of transport with chemical modification of the transported substrate; e.g., a group of bacterial transporters, termed "enzymes II" by Kundig and Roseman (1971), catalyze the uptake of carbohydrates concomitant with their phosphorylation. They are components of the bacterial phosphotransferase system (PTS).[1] The PTS transporters consist of three functional units, termed IIA, IIB, and IIC, and occasionally of a fourth subunit, IID. The IIC (and IID) units are transmembrane; the IIA and IIB units are hydrophilic. IIA, IIB, and IIC can be protein subunits of a complex or domains of a multidomain protein. Two cytoplasmic proteins, termed enzyme I and HPr, sequentially transfer phosphoryl groups from phosphoenolpyruvate to the IIA units of the different transporters. The phosphoryl groups are then transferred to the IIB unit and hence to the transported substrate. In addition to its function in carbohydrate uptake, the PTS proteins play a role in the regulation of bacterial metabolism [for reviews, see Meadow et al. (1990), Erni (1992), and Postma et al. (1993)].

The mannose transporter of *Escherichia coli* mediates uptake with concomitant phosphorylation of mannose and related hexoses that differ by substituents at the C(2) atom. It is a complex of three protein subunits termed $IIAB^{Man}$, IIC^{Man}, and IID^{Man}. IIC^{Man} and IID^{Man} are presumed to span the membrane 6 and 2 times, respectively (Erni et al., 1987). $IIAB^{Man}$ is a water-soluble peripheral membrane protein which exists as a homodimer (subunit M_r 35 016). It is associated to the transmembrane subunits on the inner surface of the membrane. $IIAB^{Man}$ consists of 2 domains, IIA^{Man} (14 kDa) and IIB^{Man} (20 kDa), which are linked by a 20-residue-long, Ala- and Pro-rich hinge (Erni, 1989). $IIAB^{Man}$ transfers phosphoryl groups from HPr to the transported substrate in the order HPr (His-15) → IIA (His-10) → IIB (His-175) → mannose (O-6′). In this reaction, the proteins are transiently phosphorylated at the indicated histidines. Phosphoryl transfer in the $IIAB^{Man}$ dimer occurs between IIA and IIB domains on the same as well as on different subunits (Stolz et al., 1993). The IIA domain provides the intersubunit contact of the $IIAB^{Man}$ dimer, and the IIB domain interacts with the transmembrane subunits (Erni et al., 1989). Highly similar to the mannose transporter (40–65% identical residues) are the fructose transporter of *Bacillus subtilis* (Martin-Verstraete et al., 1990) and the sorbose transporter of *Klebsiella pneumoniae* (EMBL Data Base Accession No. X66059, submitted by U. F. Wehmeier; Wöhrl & Lengeler, 1990). However, in contrast to $IIAB^{Man}$, IIA and IIB of these complexes exist as independent protein subunits which are not linked by an Ala-Pro-rich hinge.

† This study was supported by Grant 31-29795.90 from the Swiss National Science Foundation (B.E.), Grants Er 147/1-2, Ke 147/21, and Ke 147/23 from the Deutsche Forschungsgemeinschaft and contributions from the Fond der Chemischen Industrie (H.K.), the Sandoz-Stiftung, Basel (B.E.), and the Central Laboratories of the Swiss Red Cross, Bern (B.E.).

* To whom correspondence should be addressed.

‡ Present address: PH-AQ-F BAYER, Aprater Weg, 42111 Wuppertal, FRG.

§ Technische Universität München.

‖ Universität Bern.

⊥ Phillips Universität Marburg.

® Abstract published in *Advance ACS Abstracts,* April 1, 1994.

[1] Abbreviations: PTS, phosphoenolpyruvate–sugar phosphotransferase system; $IIAB^{Man}$, cytoplasmic subunit of the mannose transporter; IIC^{Man} and IID^{Man}, transmembrane subunits of the mannose transporter; *manX*, *manY*, and *manZ*, genes encoding $IIAB^{Man}$, IIC^{Man}, and IID^{Man}, respectively; IIA^{Glc}, cytoplasmic subunit or domain of the glucose transporter; IIA^{Mtl}, cytoplasmic domain of the mannitol transporter; HPr, histidine-containing phosphocarrier protein of the PTS; IPTG, isopropyl β-thiogalactoside; NMR, nuclear magnetic resonance; 2D, 3D, and 4D, two, three, and four dimensional; NOESY, nuclear Overhauser enhancement and exchange spectroscopy; HSQC, heteronuclear single quantum correlation; HMQC, heteronuclear multiple quantum correlation; INEPT, insensitive nuclei enhanced by polarization transfer; TPPI, time-proportional phase increment; COSY, correlation spectroscopy; TOCSY, total correlation spectroscopy.

0006-2960/94/0433-7174$04.50/0

IIAB^{Man} is a promising candidate for the study of inter-domain, intersubunit, and heterologous protein–protein interactions, and of the effect of multiple protein phosphorylation on protein conformation. Advanced knowledge of its structure might be of help for the elucidation of the structure of the membrane–protein complex. As of bacterial origin, the protein can be modified by site-directed mutagenesis, and structural alterations can be correlated with changes of function *in vitro* and *in vivo* (Stolz et al., 1993). Although the intact IIAB^{Man} dimer is too large for NMR studies in solution, the isolated domains are of a size amenable to isotope-edited NMR analysis. IIA and IIB domains can be prepared from purified IIAB^{Man} by limited trypsin digestion or be overexpressed separately (Erni et al., 1989). The separate domains are completely stable and retain their catalytic function.

Of the PTS proteins, the structures of the 9-kDa HPr of *E. coli* and *B. subtilis* have been studied in greatest detail by both NMR (Klevit & Waygood, 1986; Hammen et al., 1991; Sharma et al., 1993; van Nuland et al., 1992; Wittekind et al., 1992; van Dijk et al., 1990, 1992; Kruse et al., 1993; Kalbitzer & Hengstenberg, 1993) and X-ray techniques (El Kabbani et al., 1987; Herzberg et al., 1992; Jia et al., 1993a,b). The NMR and X-ray structures of the 18-kDa *E. coli* IIA^{Glc} subunit and of the *B. subtilis* IIA^{Glc} domain of the respective glucose transporters have also been determined (Pelton et al., 1991a,b, 1992, 1993; Worthylake et al., 1991; Fairbrother et al., 1991a,b, 1992; Liao et al., 1991; Chen et al., 1993a,b). More recently, the secondary structures of the IIA^{Mtl} domain of the *E. coli* mannitol transporter (Kroon et al., 1993) and of the IIB^{Glc} domain of the *E. coli* glucose transporter (Grdadolnik et al., 1994) have been determined by heteronuclear NMR. The IIA^{Man} and the IIA^{Mtl} domains have been crystallized (Génovésio-Taverne et al., 1990; Lammers et al., 1992).

As a first step toward elucidation of the three-dimensional structure of IIAB^{Man} by NMR, the secondary structure of the IIA domain has been determined by two-, three-, and four-dimensional NMR experiments involving ^{15}N-, ^{13}C-, and (^{15}N, ^{13}C)-labeled IIA dimers.

EXPERIMENTAL PROCEDURES

Construction of an Expression Plasmid. The recombinant plasmid pTSL2 (Erni et al., 1987) contains the *manX* gene including the noncoding region with the endogenous promotor and part of the *manY* gene. Plasmid pTSL2 was opened with *Nru*I in the 5′ noncoding region of *manX* and progressively truncated by digestion with ExoIII nuclease for different time intervals, trimmed with S1 nuclease, and digested with *Pvu*I. The *manX*-containing DNA fragments of decreasing length were purified by agarose gel electrophoresis and inserted behind the *tacP* promoter of the expression vector pJF119EH (Fürste et al., 1987) opened with *Sac*I and *Pvu*I. *E. coli* WA2127-(*manXYZ*) harboring plasmid pTSPM6 (encoding *manYZ* and kanamycin resistance; Erni et al., 1989) was transformed with the ligation mixture and plated on McConkey indicator plates containing 0.4% mannose and ampicillin. Transformants harboring recombinant plasmids with *manX* under control of *tacP* were selected and characterized as follows (de Meyer, 1992). (i) Colonies which weakly fermented mannose on the master plate (because of the leakiness of the *tacP* promotor) were transferred to IPTG-containing indicator plates. Colonies which strongly fermented mannose in the presence of 10 μg/mL IPTG were selected. (ii) IPTG-dependent overexpression of IIAB^{Man} was quantitated by Western blot analysis of lysates from cell cultures grown in liquid medium and induced in mid-log phase with 1 mM IPTG.

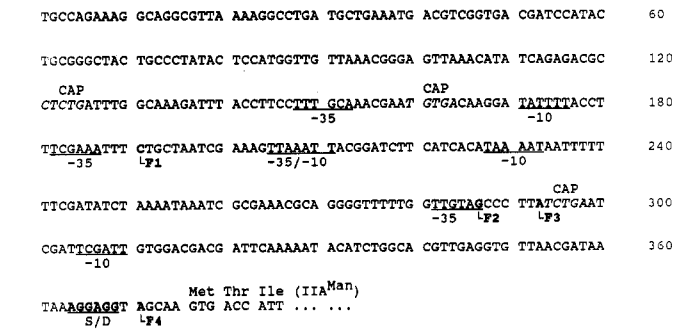

FIGURE 1: Upstream nucleotide sequence of *manX*. The nucleotides to which the *tacP* promotor of the expression vector pJF119EH (Fürste et al., 1986) was fused are indicated F1–F4. Fusions F2 and F3 are inducible, F1 is constitutive, and F4 is inactive. The four putative σ^{70} promotor sequences are *underlined*. Their homology scores calculated according to Mulligan et al. (1984) vary between 50% and 60% of the consensus sequence. Putative CAP sites are indicated in *italics*. Their homology scores calculated according to de Crombrugghe et al. (1984) vary between 67% and 71% of the consensus sequence. S/D, putative ribosome binding site. Met Thr Ile, amino-terminal residues of the IIA^{Man} domain.

(iii) Plasmids were isolated from transformants exhibiting different levels of IIAB^{Man} expression upon induction with IPTG, and the fusion joins between the *tacP* promoter and the 5′ noncoding region of *manX* were identified by DNA sequencing (Figure 1). Of the plasmids supporting maximal overexpression, pTACL293 with the fusion join closest to the translation start (83 nucleotides upstream of GUG) was used.

Sample Preparation. E. coli K-12 W3110 (*hsdR*$^+$ *hsdM*$^+$ *F′lacI*^{q} M15*pro*$^+$) harboring plasmid pTACL293 was grown in 1 L of M9 minimal medium containing either 0.1% $^{15}NH_4Cl$ (CIL, Cambridge Isotope Laboratories, Woburn, MA) and 0.6% unlabeled glucose, or 0.2% uniformly ^{13}C-labeled glucose (CIL) and unlabeled NH_4Cl, or 0.1% $^{15}NH_4Cl$ and 0.2% uniformly ^{13}C-labeled glucose. Expression of IIAB^{Man} was induced with 0.5 mM IPTG in late-log phase (OD_{600} = 1.2). The cells were harvested by centrifugation 18 h after induction.

The cells (6 g wet weight per 1 L) were resuspended in 12 mL of buffer A (20 mM NaP_i, pH 7.0, 1 mM EDTA, and 0.5 mM DTT) and ruptured by two passages through a French pressure cell (20 000 psi). The cell debris was removed by low-speed centrifugation (12000*g*, 10 min), and the membrane fraction was removed by ultracentrifugation (226000*g*, 90 min). The supernatant containing IIAB^{Man} was carefully withdrawn. The pellet was resuspended in 6 mL of buffer A followed by ultracentrifugation in order to recover the residual, membrane-associated IIAB^{Man}. The cytoplasmic supernatant and the membrane wash were combined, protamine sulfate was added to a final concentration of 0.33%, the precipitate was removed by centrifugation, and the supernatant containing IIAB^{Man} was applied to a phosphocellulose column (Whatman P11, 70-mL bed volume) equilibrated with buffer A. IIAB^{Man} was eluted with a NaCl gradient in buffer A. IIAB^{Man} elutes with 0.25 M NaCl. It was concentrated by ammonium sulfate precipitation (80% saturation). The ammonium sulfate pellet was resuspended in 2 mL of buffer A and dialyzed against the same buffer. IIAB^{Man} was cleaved with trypsin (1.7 μg of trypsin/mg of IIAB^{Man}) in buffer A (1 mg of IIAB^{Man}/mL, final volume 6 mL) at 37 °C for 30 min. The reaction was stopped with PMSF (5 μg/mL), and the reaction mixture was immediately applied to a phosphocellulose column (70-mL bed volume, equilibrated with buffer A). The IIA domain does not bind to phosphocellulose; the IIB domain was eluted with a NaCl gradient in buffer A. When necessary, the IIA domain was further purified by gel filtration (HiLoad 16/60

Superdex 75, Pharmacia). IIA and IIB were concentrated by dialysis against ammonium sulfate; the protein pellets were redissolved in buffer A, dialyzed against buffer A, and concentrated to 2 mM final protein concentration (0.2–0.5-mL end volume) with a Centricon 10 microconcentrator (Amicon). Samples were exchanged into NaP_i-buffered 100% D_2O by three cycles of dilution and concentration with a Centricon. The final yields from 1 L of cell culture were 10–15 mg of IIA and 5–10 mg of IIB.

NMR Spectroscopy. NMR experiments were carried out on a Bruker AMX-600, equipped with a multichannel interface and a 5-mm triple-resonance probehead with shielded gradients without any modifications. Some of the double-resonance ^{13}C–^1H correlations were recorded on a Bruker AMX-500, using an inverse-detection broadband probehead. All heteronuclear measurements were carried out at 37 °C at monomer concentrations of 2 mmol (U-^{13}C, ^{15}N sample, 9:1 H_2O/D_2O), 1 mmol (U-^{13}C sample, D_2O), and 2.2 mmol (U-^{15}N sample, 9:1 H_2O/D_2O). 3D HNCA (Farmer et al., 1992), HNCO (Grzesiek & Bax, 1992a), and HN(CO)CA (Bax & Ikura, 1991) spectra were recorded with pulse sequences similar to those described in the literature. Number of points, acquisition times, and measurement times, respectively, for each of the experiments are as follows: for HNCA, ^{15}N (F1), 64 real points, 32 ms; $^{13}C^{\alpha}$ (F2), 128 real points, 11.5 ms; ^1H (F3), 512 complex points, 73.7 ms, 64 scans for each increment (total measuring time 6 days); for HNCO, ^{15}N (F1), 64 real points, 32 ms; $^{13}C'$ (F2), 128 real points, 11.5 ms; ^1H (F3), 512 complex points, 16 scans per increment (36 h); for HN(CO)CA, ^{15}N (F1), 64 real points, 32 ms; $^{13}C^{\alpha}$ (F2), 128 real points, 11.5 ms; ^1H (F3), 512 complex points, 32 scans per increment (70 h). HN(CA)H (Clubb et al., 1992; Seip et al., 1992a) was recorded with ^1H (F1), 64 real points, 23.3 ms, ^{15}N (F2), 64 real points, 23.3 ms, and H^N (F3), 512 complex points, 61.5 ms. A total of 64 scans were taken (measurement time 4.5 days). HCCH-COSY (Ikura et al., 1991) [64 (^1H) × 32 (^{13}C) × 512 (^1H) complex points, 32 scans each, measurement time 3 days], HCCH-TOCSY (Bax et al., 1990) (128 × 96 × 512 complex points, 32 scans each, measurement time 5 days), and HCACO experiments were recorded in D_2O, using the U-^{13}C sample. HCACO was performed with CT-C^{α} evolution (Powers et al., 1991) [32 (^{13}C) × 64 (^1H) × 512 (^1H) complex points, 16 scans, measurement time 2 days]. A H(N)CACO (Seip et al., 1993) [48 (C') × 32 (C^{α}) × 512 (^1H) complex points, 64 scans, measurement time 4 days] spectrum was recorded with spectral widths and resolution identical to those used for the already mentioned spectra. 2D NOESY spectra were recorded at 310 and 320 K with different mixing times.

A ^{15}N-separated 3D NOESY was recorded with jump–return water suppression and a 100-ms mixing time; 192 real points were taken in the indirect ^1H dimension (F1). The F2 (^{15}N) and F3 (^1H) acquisition parameters were identical to those used in all other correlations (vide supra); 16 scans were taken, resulting in a total measurement time of 5.5 days. A CBCA(CO)NH spectrum was recorded (Grzesiek & Bax, 1992b) with 160 real points in F1 (C^{α}/C^{β}, spectral width of 12 500 Hz) and 64 scans per increment (F2, ^{15}N, 56 real points, 23 ms; F3 ^1H, 512 complex points, 55 ms, measurement time 5 days). A HCA(CO)N (Kay et al., 1990b; Powers et al., 1991) spectrum in H_2O was recorded, with constant time evolution of fully refocused CA magnetization and water suppression using pulsed field gradient echo. To compensate for the Bloch–Siegert phase errors during CA coherence caused by C' decoupling, additional C' 180° pulses were placed immediately before the first 90° C' pulse and before the last 90° CA pulse (Vuister & Bax, 1992). A ^{15}N–^{13}C-separated 4D NOESY (Kay et al., 1990a) was recorded (50-ms mixing time) with 64 complex points in F1 (^1H), 16 complex points in F2 (^{13}C), 32 real points in F3 (^{15}N), and 512 real points in F4 (H^N). A total of 16 scans were taken for each increment (measurement time 6 days). Spectral widths were identical to those used in CBCA(CO)NH. The spectral width in the (F1) proton dimension was set to 6 ppm. For the ^{15}N dimension, a single quantum evolution (HSQC) was chosen, instead of the HMQC as described in the literature. In addition to the slightly higher sensitivity, the HSQC sequence offers an easy method for water suppression using a spin-lock pulse at the end of both INEPT transfers (Messerle et al., 1989). This removes the necessity of saturation of the water resonance and therefore allows for the observation of labile amide protons.

Quadrature detection in all experiments was achieved using either the TPPI or the States–TPPI method for frequency discrimination in the indirectly recorded dimensions. To yield identical phase properties for folded and unfolded peaks in the indirect dimensions, either delays were set to the correct values to obtain 180° and −360° phase correction for zero order and first order, respectively, or an additional 180° refocusing pulse was applied in single quantum evolution periods (Schmieder et al., 1991). Postacquisitional water suppression was performed by subtraction of a polynomial from the FID (Marion et al., 1989). Additional base-line flattening was achieved by subtraction of a series of sines and cosines that were fitted iteratively to the base line. Spectra were processed using commercially available software (FELIX program, Hare Research). The heavily truncated interferograms in the indirect dimensions of the 4D experiment (16 complex ^{13}C and ^{15}N) were extrapolated by linear prediction to 32 complex points respectively.

RESULTS AND DISCUSSION

Overexpression of $IIAB^{Man}$ and Sample Preparation. To optimize protein expression and to minimize the risk of plasmid loss during fermentation, the *manX* gene was put under the control of the inducible *tacP* promotor. The optimal distance between *tacP* and the coding region of *manX* was determined empirically by progressively truncating the noncoding region between *tacP* and the translation start. The fusion joins of four promotor fusions (F1–F4) were identified (Figure 1). Fusions of *tacP* to nucleotides 287 (F2) and 293 (F3) resulted in an IPTG-inducible gene. The fusions F2 and F3 occurred between the −10 and −35 elements of the putative σ^{70} promotor sequence closest to the start codon. The F1 fusion of *tacP* to nucleotide 191 is located between the −10 and −35 elements of the third putative σ^{70} promotor. Expression remained constitutive and could not be further stimulated with IPTG. So, the two downstream promotors appear sufficient for maximal expression. The fusion F4 of *tacP* to nucleotide 371 is inactive, possibly because the endogenous ribosome binding site is missing (Figure 1).

Due to several lysyl residues in the hinge region, limited trypsinolysis did not afford a completely homogeneous IIA protein. Electrospray mass spectrometry as well as NMR revealed three IIA species which all lacked the amino-terminal methionine and differed in their carboxy terminus (results not shown).

NMR Results: Special Spectral Features. Figures 2 and 3 show the 2D ^{15}N-HSQC and ^{13}C-HMQC spectra of IIA^{Man}, recorded with the U-^{15}N/U-^{13}C sample in H_2O. A relatively good chemical shift dispersion for some of the NH and HA protons indicative of partial β structure is apparent. The HA protons at lowest and highest field are at 6.41 and 2.51 ppm,

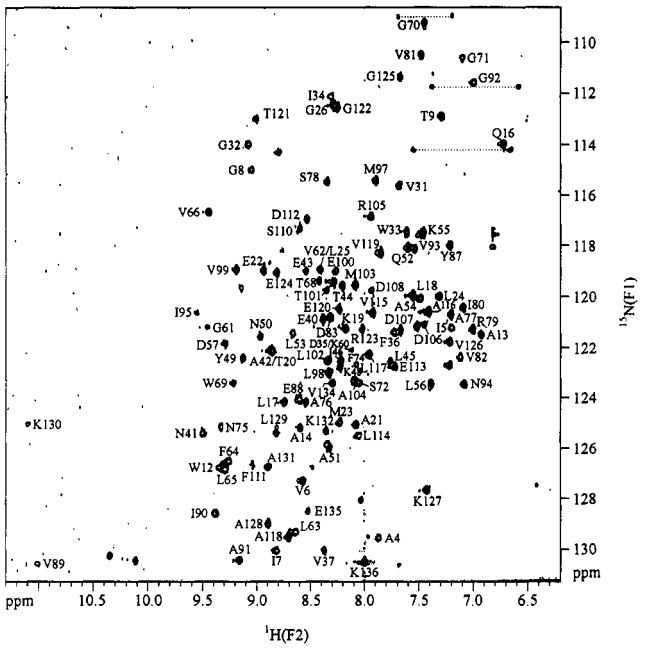

FIGURE 2: ^{1}H–^{15}N HSQC spectrum of U(^{13}C,^{15}N)-IIA^{Man} in 90% H_2O/10% D_2O at 37 °C, recorded with eight scans using gradients for water suppression. The assignments of the amide proton–nitrogen pairs have been indicated. Side chain amino group signals are marked by dotted lines.

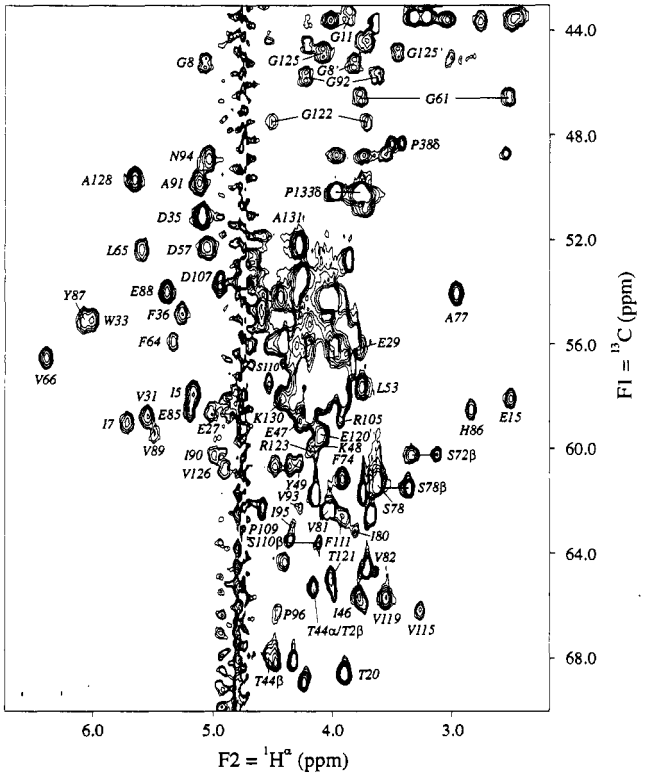

FIGURE 3: H$^\alpha$–C$^\alpha$ region of the 2D ^{1}H–^{13}C-HSQC spectrum recorded with the same sample and conditions as in Figure 2. Presaturation was applied to suppress the water resonance at 4.76 ppm. Strong overlapping resonances have not been labeled. Fast T_2 relaxation is responsible for the broad lines in both dimensions.

respectively. The amide proton chemical shift range spans from 5.17 to 11.10 ppm. It is also obvious, however, that the major part of the α-proton resonances is found in a narrow spectral region (3–4.5 ppm). Because of the homodimeric character of the protein, only 1 set of signals of 135 residues is visible. A substantial variation in line width and intensity of the resonances is visible in the ^{13}C-HMQC and ^{15}N-HSQC spectra. Especially residues 130–136 (C-terminus) give rise

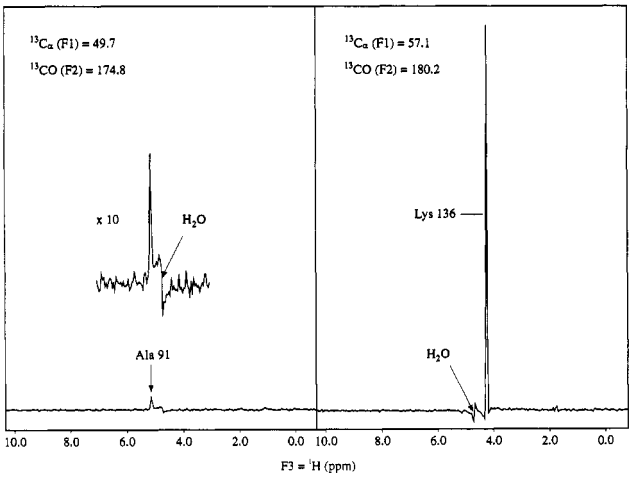

FIGURE 4: Two 1D vectors from a HCACO spectrum, extracted at the ^{13}C$^\alpha$ frequencies of A91 (left) and K136 (right) with equal scaling. Comparison of the two resonances illustrates the extensive variety of signal intensities in this spectrum due to regions of different mobility. The heights of the signals differ by about a factor of 200.

to very intense, sharp peaks in both spectra due to their greater mobility, compared to the rest of the protein. As an example, two 1D vectors taken from slices of the HCACO spectrum at carbonyl frequencies of 174.8 and 180.2 ppm are shown in Figure 4. These kinds of intense resonances disturb weaker peaks in their vicinity in many spectra. The heterogeneity of the sample, however, did not significantly affect the appearance of the spectra.

Backbone Assignment. Backbone assignment of isotopically enriched proteins is usually based on the combination of connectivities observed in triple-resonance experiments. Because of the high molecular mass (31 kDa) of labeled IIA^{Man}, only the most sensitive [HNCA, HNCO, HN(CO)CA, HCACO, HN(CA)H, and CBCA(CO)NH] of the triple-resonance experiments gave useful spectra, i.e., spectra where most of the expected cross-peaks could be found. Figure 5 shows representative planes of the HCACO, HNCO, HNCA, and HN(CA)H spectra. Some of the less sensitive experiments, e.g., H(N)CACO and HCA(CO)N (both optimized for the application to large proteins), also yielded useful information, although not all possible correlations were present in these spectra. The HCCH-COSY and HCCH-TOCSY spectra were of limited value for the sequential assignment, because of severe overlap in the HA-CA region. The ^{1}H, ^{15}N, ^{13}CA, and ^{13}C′ assignments are provided in Table 1.

Several problems appear during the sequential assignment. It became obvious that some correlations were missing in most HN-X [X = CO, CA, (CA)CO, (CO)CA] spectra, partly because these spectra were recorded with water presaturation. Resonances were lost because of rapid exchange with the solvent protons (pH 7.5, temperature 37 °C). Some resonances could still not be observed, even if no presaturation was applied during the experiments. The wide range of different line widths and intensities lead to additional difficulties in the evaluation of the correlations involving CA or HA nuclei. In addition, most of the spectra show some overlap and degeneracy because of the helical content of IIA^{Man}.

Assignment Strategy. More than 60% of the sequential assignment was accomplished in a very straightforward manner, using HNCA, HNCO, HN(CO)CA, HCACO, and H(N)COCA spectra as described previously (Seip et al., 1993). During each sequential step, reference to 3D NOESY-(^{15}N)-HMQC (preferably in helical regions) and 4D (^{13}C/^{15}N)-edited NOESY (in β-sheet and loop structures) was made to confirm the assignment (Figure 6). This procedure was found

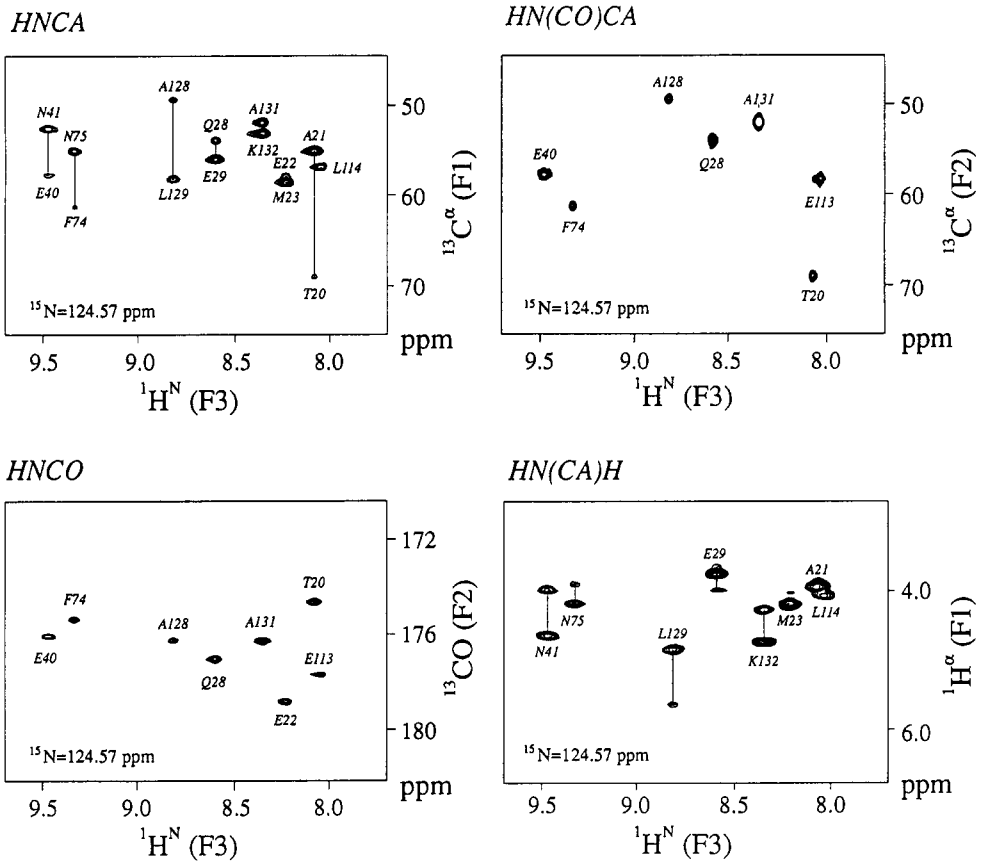

FIGURE 5: Representative planes from HNCA, HNCO, HN(CA)H, and HN(CO)CA at the same chemical shift (nitrogen at 124.57 ppm) illustrate the quality of the spectra that were used in this work. As expected, the most intense resonances were found in the HNCO and HN(CO)CA spectra. Most of the sequential correlations from HN(CO)CA could also be found in HNCA. HN(CA)H, however, shows predominantly intraresidue correlations. The M23 cross-peak is visible in an adjacent plane of the HN(CO)CA.

to be very reliable and efficient. The remaining part of the assignment work utilized the CBCA(CO)NH spectrum for identification of the amino acid residue type. Stretches of four to six residues that were found to be linked sequentially were identified unambiguously by their unique combination of CB chemical shifts. It must be noted, however, that many of the CB resonances were missing, so that a complete set of correlations could not be obtained. Another reason for the incomplete set of resonances at this stage was uncertainties in the determined peak positions. We therefore tried to complete the assignment using sequential NOEs from 2D NOESY and 3D NOESY-HMQC. To avoid possible pitfalls, inevitably associated with NOE-based sequential assignment, reference to the triple-resonance spectra was made continuously. The procedure required the assignment of the HA protons and numerous of the side chain resonances as well and made a tedious manual examination of the spectra necessary. The 2D ^{1}H–^{1}H-TOCSY shows only a fraction of the possible correlations, and HCACO was plagued by severe overlap in the HA-CA region. In particular, the leucine CA carbons show a high degree of shift degeneracy which made correlation to the corresponding HAs very difficult. Because there are only few cases where overlap occurs in the ^{1}H–^{15}N-HSQC (e.g., A21–L114, G26–G112, S72–A104), a HN(CA)H spectrum in which correlations from amide protons to both HA(i) and HA(i–1) are observed was used to resolve ambiguities and found to be an invaluable tool for establishing the HA assignment.

The remaining, "problematic" residues, that have not been assigned after the described procedure, are entirely located in loop regions (residues 28–31, 56–61, and 81–86). In many cases, missing links to these residues could be established with a HCA(CO)N experiment. The important feature of this experiment is that, unlike HN(CO)CA or HN(COCA)H (Clubb et al., 1992), correlations to nitrogens belonging to exchanging or broadened amide protons can be observed. Additionally, ^{15}N chemical shifts of all proline residues could be assigned with this spectrum. Once the ^{15}N frequency was found, reference to the well-resolved and very sensitive ^{1}H–^{15}N-HSQC yields the frequency of the corresponding H^{N} proton. In other spectra, the resonances of these amides were too weak to be observed.

Due to the highly helical nature of the protein, both 2D NOESY and 3D ^{15}N-HMQC-NOESY show a large number of $d_{NN(i,i+1)}$ connectivities between sequential amides. In cases where multiple possibilities arise or a break in the assignment using NH groups occurs, consideration of NOEs yields important information. This was the case for all glycine amide protons. The glycines, whose NH correlations are either missing or subjected to strong overlap in other spectra, could be identified unambiguously only after extensive inspection of the NOESY spectra. If any, only weak peaks could be observed for the glycine residue in either HN(CA)H or HCACO spectra. Similar difficulties arised for the threonine residues. We hope to complete the assignment during the refinement of the 3D structure.

Secondary Structure. The secondary structure of IIA^{Man} was determined by analyzing the sequential and long-range NOEs between the backbone protons. Using the resonance assignments obtained from triple-resonance experiments as described above, nonoverlapping regions of the 2D NOESY spectrum were used for qualitative determination of NOE distances. In cases where overlap prevents the unambiguous assignments in the 2D spectra, the step to higher-dimensional NOESY experiments yielded the missing information. Especially for NOEs between H^{N} protons to protons bonded to

Table 1: Backbone Assignment of the IIA Domain at pH 7.5 and 37 °C (in ppm)[a]

residue	H^N	^{15}N	H^α	$^{13}C^\alpha$	$^{13}C{=}O$	residue	H^N	^{15}N	H^α	$^{13}C^\alpha$	$^{13}C{=}O$
Thr-2	*b*	*b*	4.10	59.5	173.2	Trp-69	9.26	123.3	4.47	56.1	174.3
Ile-3	8.59	126.1	3.87	62.9	173.5	Gly-70	7.45	108.7	4.48	45.2	172.5
Ala-4	7.89	132.9	4.54	51.9	174.8	Gly-71	7.11	110.5	3.77	46.0	174.6
Ile-5	7.16	120.8	5.16	57.9	173.5	Ser-72	8.05	123.0	4.40	56.1	176.9
Val-6	8.58	127.3	4.73	59.4	173.3	Pro-73		116.3	3.71	66.5	178.3
Ile-7	8.82	130.2	5.73	59.1	174.4	Phe-74	8.09	122.6	3.91	61.2	175.3
Gly-8	9.06	114.8	5.07,3.82	45.2	170.4	Asn-75	9.34	125.1	4.20	55.3	177.4
Thr-9	7.29	112.2	5.14	58.6	172.2	Ala-76	8.54	124.0	4.01	54.3	176.5
His-10	9.87	133.3[c]	2.80	58.6	176.2	Ala-77	7.22	120.4	2.95	54.1	178.4
Gly-11	5.16	115.7	4.82,3.97	46.7	172.0	Ser-78	8.36	115.1	3.61	61.2	173.8
Trp-12	9.34	126.7	5.04	58.7	175.7	Arg-79	7.00	121.1	3.97	57.4	177.0
Ala-13	6.92	120.7	4.03	54.2	177.2	Ile-80	7.10	120.1	3.79	63.4	176.6
Ala-14	8.60	125.1	3.77	56.2	177.1	Val-81	7.49	109.9	3.98	62.4	176.9
Glu-15		117.8	2.54	58.2	177.9	Val-82	7.12	122.2	3.73	64.7	173.9
Gln-16	6.72	113.5	4.29	55.6	177.6	Asp-83	8.27[c]	120.8	4.12	56.5	176.8
Leu-17	8.75	124.1	4.04	57.9	177.2	Lys-84	8.90	118.0	4.42	53.8	174.3
Leu-18	7.48	119.8	4.08	57.5	177.0	Glu-85	7.22	121.6		54.2	
Lys-19	8.18	121.0	4.23	59.2	179.3	His-86				54.1	169.9
Thr-20	8.87	122.1	3.88	68.9	174.4	Tyr-87	7.23	117.3	6.04	55.1	174.9
Ala-21	8.08	125.1	3.94	55.2	178.7	Glu-88	8.60	123.7	5.38	53.9	172.2
Glu-22	8.94	118.7	4.26	58.0	179.3	Val-89	11.00	130.4	5.50	59.6	172.3
Met-23	8.22	124.5	4.20	58.7	176.5	Ile-90	9.38	128.7	5.00	60.1	174.1
Leu-24	7.31	119.4	4.31	56.3	177.8	Ala-91	9.19	130.5	5.12	49.7	174.8
Leu-25	8.42	118.3	4.63	54.8	177.3	Gly-92	6.99	105.4	3.56,4.22[c]	45.5	173.8
Gly-26	8.28	111.9	4.58,3.90	46.6		Val-93	7.51	117.8	4.27	62.4	171.3
Gly-26						Asn-94	7.10	122.9	5.05	48.9	172.9
Glu-27						Ile-95	9.55	120.5	4.31	63.4	173.4
Gln-28						Pro-96		123.9	4.44	66.3	175.9
Glu-29						Met-97	7.90	115.0	4.20	58.2	178.6
Asn-30			4.65	53.5	173.4	Leu-98	8.32	122.6	3.90	58.2	176.5
Val-31	7.67	115.3	5.52	59.0	174.4	Val-99	9.19	118.3	3.73	66.1	176.7
Gly-32	9.08	113.1	4.68	46.1	170.2	Glu-100	8.26	118.6	4.18	58.8	176.8
Trp-33	7.61	116.8	6.05	55.2	175.1	Thr-101	8.28	119.0	3.73	67.4	175.3
Ile-34	8.32	111.5	4.84	58.4	173.3	Leu-102	8.34	122.5	3.96	57.8	179.3
Asp-35	8.09	121.9	5.12	51.2	173.5	Met-103	8.09	119.2	4.34	58.6	178.0
Phe-36	7.73	121.2	5.28	54.9	172.5	Ala-104	8.09	123.2	4.28	53.6	179.5
Val-37	8.37	129.4	4.14	58.0	171.7	Arg-105	7.96	116.5	3.93	58.9	177.4
Pro-38		125.2	4.23	63.2	176.5	Asp-106	7.47	120.8	4.70	56.1	175.4
Gly-39	8.28	111.4	4.55,3.93	42.9	172.0	Asp-107	7.66	120.8	4.97	53.7	173.7
Glu-40	8.39	120.6	4.00	57.8	176.1	Asp-108	7.92	119.4	4.58	54.3	175.0
Asn-41	9.48	125.3	4.67	52.8	174.5	Pro-109		126.4	4.60	63.2	175.9
Ala-42	8.85	121.6[c]	3.88	55.1	178.2	Ser-110	8.60	116.9	4.52	57.5	173.8
Glu-43	8.55	118.7	4.07	59.7	178.9	Phe-111	9.02	126.7	3.88	62.7	175.7
Thr-44	8.22	119.3	4.10	65.6	175.9	Asp-112	8.52	116.5	4.39	56.8	178.9
Leu-45	7.76	122.4	3.90	57.2	177.1	Glu-113	7.72	122.4	3.95	58.3	177.6
Ile-46	8.22	122.3	3.77	65.8	176.7	Leu-114	8.04	125.4	4.07	56.9	176.8
Glu-47	7.49	120.9	4.25	59.0	179.1	Val-115	7.93	120.4	3.24	66.3	175.9
Lys-48	8.22	122.7	4.20	59.9	179.9	Ala-116	7.40	120.2	4.06	54.2	179.4
Tyr-49	9.14	122.3	4.27	60.7	177.8	Leu-117	7.94	122.1	4.24	57.4	178.6
Asn-50	8.99	121.4	4.67	55.9	177.5	Ala-118	8.70	129.1	3.85	55.6	178.6
Ala-51	8.31	125.9	4.31	54.3	179.8	Val-119	7.84	118.2	3.54	65.9	176.5
Gln-52	7.60	117.7	4.07	57.1	177.8	Glu-120	8.24	120.2	4.08	59.4	178.6
Leu-53	8.68	121.2	3.74	57.8	177.5	Thr-121	8.99	112.5	4.00	66.8	178.5
Ala-54	7.55	119.7	4.25	53.4	177.6	Gly-122	8.24	111.9	4.57,3.74	47.3	173.9
Lys-55	7.47	117.2	4.57	55.2	174.9	Arg-123	8.03	121.1	4.11	60.0	178.0
Leu-56	7.39	123.3	4.73	52.9	174.2	Glu-124	8.83	118.8	4.10	57.0	176.7
Asp-57	9.29	121.9	5.10	52.5	177.1	Gly-125	7.70	105.7	4.09,3.43	44.9	171.8
Thr-58	8.76	117.2				Val-126	7.20	122.1	4.89	60.8	174.1
Thr-59					173.2	Lys-127	7.43	127.0	4.61	54.9	172.8
Lys-60	8.09	121.8[c]	4.82	58.8	176.8	Ala-128	8.90	128.7	5.68	49.7	176.3
Gly-61	9.46	121.2[c]	3.77,2.52	45.2	171.5	Leu-129	8.82	125.3	4.87	57.9	177.1
Val-62	8.36	119.0	4.47	60.6	172.2	Lys-130	11.10	124.5	4.42	57.6	178.3
Leu-63	8.63	129.4	5.04	52.3	173.8	Ala-131	8.89	126.4	4.29	52.2	176.3
Phe-64	9.26	125.8	5.37	55.8	173.5	Lys-132	8.35	125.2	4.75	53.4	173.8
Leu-65	9.29	126.8	5.61	52.3	175.3	Pro-133		122.5	4.62	61.6	175.9
Val-66	9.45	116.4	6.41	56.5	176.0	Val-134	8.31	123.4	4.14	61.9	175.1
Asp-67	8.29	119.9	4.41	60.6	175.8	Glu-135	8.52	128.7	4.42	55.9	174.3
Thr-68	8.41	119.3	4.00	65.8	175.5	Lys-136	8.00	130.5	4.26	57.1	180.2

[a] ^1H and ^{13}C chemical shifts relative to 3-(trimethylsilyl)propionate-d_4 sodium salt (TSP). ^{15}N chemical shifts are referenced relative to $^{15}NH_4Cl$. [b] Not observed. [c] Tentative assignment.

carbon, ambiguities arising from degenerate proton chemical shifts could be resolved with additional reference to its carbon frequency in the 4D NOESY. The obtained NOEs from the different 2D, 3D, and 4D spectra are denoted in Figure 7. These NOESY spectra were recorded with relatively long mixing times (60–100 ms) for sensitivity reasons. Forthcoming distance geometry calculations will be performed only with data from NOESY spectra with short mixing times to avoid errors caused by spin diffusion. For the β-sheets, almost all $H^N(i)$–$HA(i-1)$ were found to be more intensive than the

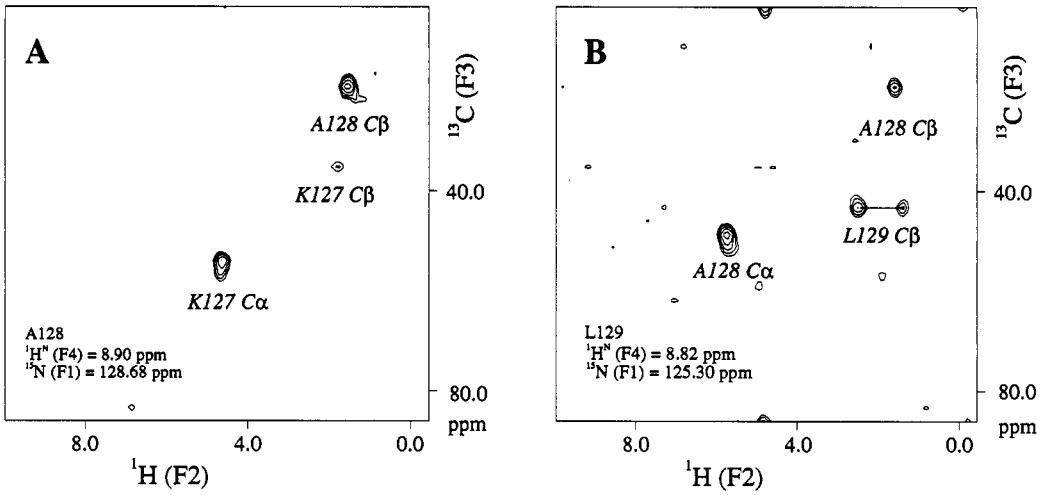

FIGURE 6: Two representative 2D planes from the 4D $^{13}C/^{15}N$-edited NOESY, taken at the $^{15}N/^1H^N$ shift of Ala-128 (A) and Leu-129 (B). The reuslting $^1H(F2)$–$^{13}C(F3)$-HMQC slices contain only cross-peaks of carbon-bonded protons, which show an NOE to the specified H^N in F4.

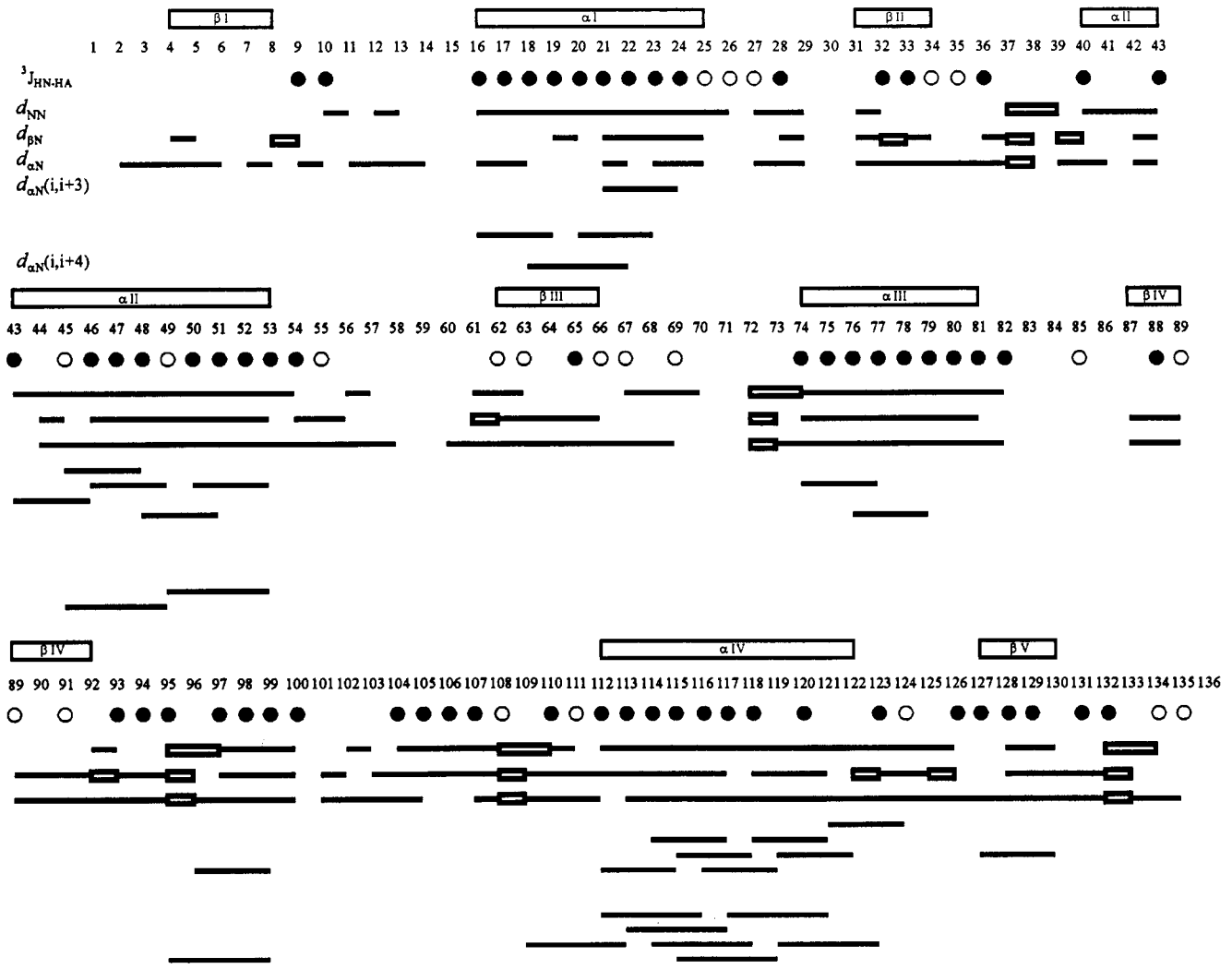

FIGURE 7: Summary of the sequential and medium-range NOE connectivities for IIA^{Man}. The relative sizes of the NOEs have not been distinguished. $^3J_{HN-HA}$ smaller than 4 Hz are represented by filled circles and $^3J_{HN-HA} > 6$ Hz by opened circles. Opened boxes indicate segments for which the given sequential connectivity is not possible (proline and glycine). The identified secondary structure elements are shown along the sequence.

$H^N(i)$–$HA(i)$. For the helical regions, all $H^N(i)$–$H^N(i-1)$ cross-peaks could be assigned. Most long-range NOEs were found for helix IV (Figure 8). Measured $^3J_{HN-HA}$ coupling constants (Seip et al., 1992b) are in good agreement with the secondary structure derived by NOEs.

The β-sheet was identified by the interstrand NOEs, shown in Figure 9. Amide protons, which had not exchanged after more than 1 year in the D_2O sample, are indicated by circles in Figure 9. With the exception of seven residues, located in the helices, all residues not exchanging H^N protons are located

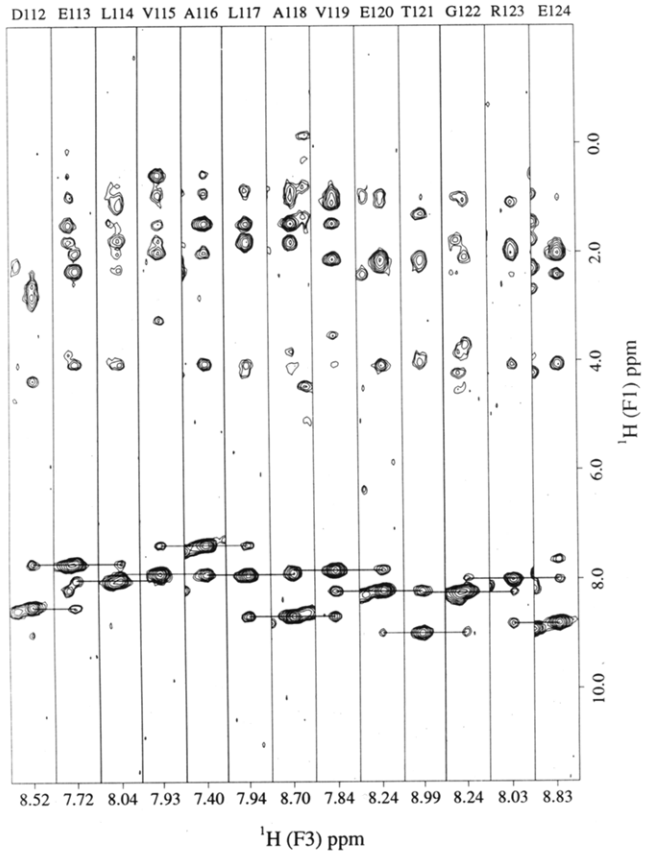

FIGURE 8: NOESY stripes at different ^{15}N chemical shifts taken from 3D ^{15}N-NOESY-HMQC of helix IV (residues 112–124). Sequential NH(i+1)–NH(i)–NH(i–1) cross-peaks, typical for helices, are connected by lines.

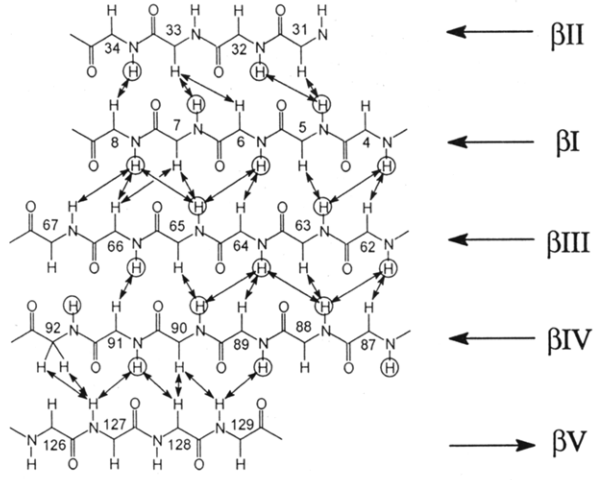

FIGURE 9: β-Sheet topology of IIA^{Man} as derived from NMR data. Arrows represent interstrand NOEs observed in 2D NOESY [$d_{\alpha\alpha}(i,j)$, $d_{\alpha N}(i,j)$, $d_{NN}(i,j)$], 3D ^{15}N-NOESY-HSQC [$d_{\alpha N}(i,j)$, $d_{NN}(i,j)$], and 4D ^{13}C,^{15}N-edited NOESY [$d_{\alpha N}(i,j)$]. Amide protons shown in circles did not exhibit any exchange with the solvent.

in β-sheets. They are considered to be involved in hydrogen bonds, which confirms the proposed secondary structure. Most of the sheet protons resonate at a remarkable low-field shift, so that there is almost no overlap in the 2D NOESY (Figure 10). The first four sheets are orientated parallel. The helices between these sheet strands cross the β-sheet. For helix IV (Asp-112–Gly-122) between the antiparallel sheets IV (Tyr-87–Gly-92) and V (Lys-127–Lys-130), no prediction is possible with the data analyzed so far.

The secondary structure is further confirmed by the CA chemical shifts. In Figure 11, deviations of the CA shifts from random-coil values for each residue are plotted. β-Sheets

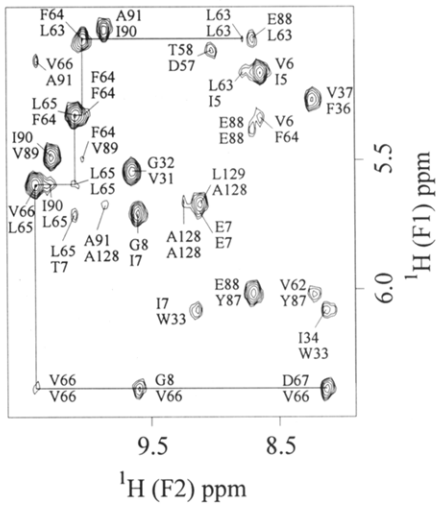

FIGURE 10: Low-field HN-HA section from the two-dimensional NOESY spectrum recorded at 37 °C. The lines mark intra- and interresidual NOE connectivities for βIII (Val-62–Val-66). Additional interstrand NOEs to βI and βIV, respectively, are labeled. Upper labels correspond to H^N (F2) and lower labels to HA (F1).

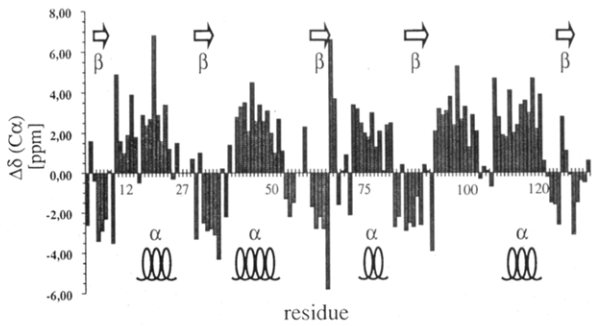

FIGURE 11: Deviations $\Delta\delta$(CA) of CA chemical shifts from random-coil values for each amino acid residue. A series of negative values correspond to β-structure, while helices are characterized by multiple consecutive positive values.

are indicated by a theoretical deviation $\Delta\delta$(CA) of –1.5 ppm, helical regions around 3 ppm (Spera & Bax, 1991). A good correlation was found.

CONCLUSIONS

The IIA domain of the IIAB^{Man} subunit forms a stable dimer of 28-kDa dimeric molecular mass. The IIA^{Man} dimer is thus at the upper molecular mass limit for NMR analysis. However, long-term stability of the dimer at elevated temperatures (up to 45 °C) and the application of novel procedures developed for medium-sized proteins (Grzesiek & Bax, 1992a,b; Seip et al., 1992a,b, 1993) allowed almost complete backbone assignment and secondary structure determination. The sequential and long-range NOEs show that the IIA domain contains a β-sheet structure (Figures 9 and 12) of four parallel and one antiparallel strand and that the strands are connected by four helical segments. The β-strand order is V IV III I II (Figure 9). Assuming an open sheet structure and that the β–α–β motifs are right-handed (Branden & Tooze, 1991), helices II and III and helix I must be packed against opposite sides of the β-sheet. The loops 1 and 3 connecting β-strand I to α-helix I and β-strand III to α-helix III form a topological switch point. According to the postulate of Branden (1980), that the active sites in α/β proteins are at topological switch points, loops 1 and 3 of IIA^{Man} should contain the active-site residues. On the basis of the NMR-derived secondary structure, a 3D model of the IIA domain was constructed by Markovic-Housley et al.

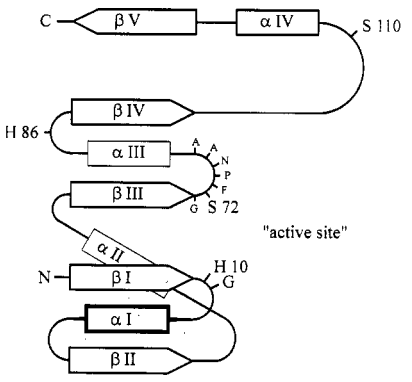

FIGURE 12: Hypothetical open twisted sheet topology of the IIA domain. His-10 is the phosphorylated residue in the active site. The strictly conserved residues of the active site at the topological switch point are indicated. His-86 is important for phosphoryl transfer from His-10 to His-175 on the IIB domain. IIA truncated at Ser-110 was found to retain *in vivo* activity (see text for details).

(1994) using tertiary structure prediction methods and the known atomic structure of clostridial flavodoxin. The NMR results confirm the β-strand order IV III I II (residues 1–120) of the predicted 3D structure, with the exception of β-strand V (residues 127–130) which is antiparallel in IIA^{Man} but parallel in flavodoxin.

The following properties of IIA^{Man} are compatible with an open sheet topology as depicted in Figure 12. His-10 is the phosphorylated residue in the active site of IIA^{Man} (Erni et al., 1989). In addition to His-10, Ser-72 is also essential for IIA function (Stolz et al., 1993). Heterodimers between H10C and S72C mutants are inactive. Similarly, mixtures of the $IIAB^{Man}$ mutant W12F with S72C and of W12F with H10C are noncomplemeting (Stolz et al., 1993). This indicates that all three residues are part of a single functional unit within a IIA monomer, that is the active site formed by loops 1 and 3 (Figure 12). In contrast and for comparison, interallelic complementation did occur between the H10C and H86N mutants, suggesting that His-10 and His-86 belong to different functional units. As shown in Figure 12, His-10 and His-86 are in loops on opposite edges of the sheet. The amino acid sequence alignment between the IIA^{Man} domain and the structurally related LevD and SorF subunits of the *B. subtillis* fructose transporter (Martin-Verstraete et al., 1990) and the *K. pneumoniae* sorbose transporter (EMBL Data Base Accession No. X66059, submitted by U. F. Wehmeier; Wöhrl & Lengeler, 1990) further highlights the functional importance of loops 1 and 3. The GS/TPXNAA (X, aromatic residue) motif of loop 3 and the conserved His-10 and Gly-11 residues in loop 1 are the most strongly conserved elements of the three homologous proteins. α-Helix IV and β-strand V might not be absolutely necessary for IIA function. Chromosomally encoded IIA^{Man}, truncated after Ser-110, conferred PTS activity *in vivo*, if the IIB^{Man} domain, IIC^{Man}, and IID^{Man} were coexpressed from a plasmid. $IIB^{Man}/IIC^{Man}/IID^{Man}$ had no PTS activity in a host from which IIA^{Man} was completely deleted (Erni, unpublished observation). Helix IV and β-strand V might already be a part of the interdomain linker and be dispensable as a structural component of the IIA domain.

The IIA domain makes different protein–protein contacts. If forms very stable homodimers (Erni et al., 1989; Markovic-Housley et al.)[2] and binds to HPr and the IIB domain between which it relays phosphoryl groups. Phosphorylation of His-10 increases the extent of dimerization (observed on SDS–polyacrylamide gels; Erni et al., 1989) while its substitution by cysteine or asparagine prevents dimerization. The stability of the dimer in SDS is pH-dependent with a transition from stable to unstable between pH 7.0 and 6.5 (Erni, unpublished observation). His-10 could thus be part of the contact site or affect dimerization indirectly by inducing conformational changes. His-86 is important for phosphoryl transfer between His-10 of the IIA and His-175 of the IIB domain but not for phosphorylation of IIA by HPr (Stolz et al., 1993). His-86 and His-175 mutants have identical phenotypes and do not complement each other; i.e., heterodimers between a H86N mutant and a H175C mutant are inactive. The two residues must be present on the same subunit. This suggests that His-86, although located in the IIA domain, functionally belongs to the active site of the IIB domain and that it might be at or close to the interface between the IIA and IIB domains.

All PTS proteins are transiently phosphorylated at either histidine (enzyme I, HPr, IIA units, IIB unit of the mannose transporter) or cysteine [IIB domains of the transporters from mannitol and glucose; reviewed in Postma et al. (1993)]. How similar are their folding topologies and active sites? HPr is a four-stranded β-sheet with three α-helices packed on top of the β-strands. The active center is in a loop between β-strand I and α-helix I. The phosphate is bound to His-15 and stabilized by interactions with the guanidinium group of Arg-17 and main chain amide groups of Ala-16 and Arg-17. It might be stabilized by the N-terminal dipole of α-helix I. His-15 and Arg-17 are invariant in all HPr (Jia et al., 1993a,b). IIA of *E. coli* and *B. subtilis* have 42% sequence identity. They are antiparallel β-sheet sandwiches or β-barrels with six strands on either face. The two structures differ with respect to the exact number, length, and topology of the β-strands. The phosphate is covalently bound to His-90 (*E. coli*; His-83 *B. subtilis*) at the C-terminus of a β-strand and stabilized by hydrogen bonding to His-70 (*E. coli*; His-68 *B. subtilis*) at the N-terminus of an adjacent strand and within a distance of 3.3 Å (Worthylake et al., 1991; Pelton et al., 1993). This second His was shown to be important for transfer of the phosphoryl group to the IIB domains but not for phosphorylation of IIA by HPr (Presper et al., 1989; Reizer et al., 1992). The two His are invariant in all IIA domains of the transporters belonging to the glucose family [reviewed in Postma et al. (1993)]. The IIA^{Mtl} domain differs from the IIA^{Glc} units in sequence and secondary structure. It is predominantly α-helical with only two β-strands. In addition to the phosphorylated histidine (His-554, *E. coli*), a second histidine and one arginine are invariant in the IIA domains belonging to the mannitol family of transporters (Kroon et al., 1993). However, the function of these residues has not yet been examined. The IIB domain of the glucose transporter ($IICB^{Glc}$) consists of four β-strands forming an antiparallel β-sheet and three α-helical segments (Grdadolnik et al., 1994). The active-site cysteine is at the C-terminus of β-strand I ($\alpha\beta_{Cys421}\beta\alpha\beta\beta\alpha$). The IIA^{Man} domain of the mannose transporter differs from the IIA and IIB domains described above with respect to sequence and secondary and quaternary structure. It has an α/β structure which is predicted to fold into an open twisted sheet. Invariant are the phosphorylated histidine in one loop and the sequence GS/TPXNAA (X: aromatic residue) in the second loop of the active center (Figure 12). However, no arginine (as in HPr) or second histidine (as in the other IIA domains) is conserved in the homologous IIA^{Man}, SorF, and LevD proteins. In conclusion, although all IIA domains are phosphorylated by the same HPr protein, the structures of their phosphorylation sites and the molecular mechanism of phosphoryl transfer are likely to be dissimilar.

[2] Markovic-Housley, Z., Cooper, A., Lustig, A., Flükiger, K., Stolz, B., & Erni, B. (1994) *Biochemistry* (submitted for publication).

It will be of interest to examine which properties enable HPr to bind to the different IIA domains (Herzberg, 1992; van Nuland et al., 1993; Chen et al., 1993a). Structural refinements and further NMR studies are in progress to elucidate the three-dimensional structure of the IIA^{Man} domain, the structural changes which are induced by phosphorylation, and the protein–protein interactions within the IIA dimer.

ACKNOWLEDGMENT

We thank Dr. C. M. Dobson for the ES-MS spectrum of [U-^{15}N]IIA^{Man} and Dr. Markovic-Housley for helpful discussions.

REFERENCES

Bax, A., & Ikura, M. (1991) *J. Biomol. NMR 1*, 99–104.
Bax, A., Clore, G. M., & Gronenborn, A. M. (1990) *J. Magn. Reson. 88*, 425–431.
Branden, C. (1980) *Q. Rev. Biophys. 13*, 317–388.
Branden, C., & Tooze, J. (1991) in *Introduction to Protein Structure*, pp 43–51, Garland Publishing, Inc., New York.
Chen, Y., Reizer, J., Saier, M. H., Fairbrother, W. J., & Wright, P. E. (1993a) *Biochemistry 32*, 32–37.
Chen, Y., Fairbrother, W. J., & Wright, P. E. (1993b) *J. Cell. Biochem. 51*, 8232–8237.
Clubb, R. T., Thanabal, V., & Wagner, G. (1992) *J. Biomol. NMR 2*, 203–210.
de Crombrugghe, B., Busby, S., & Buc, H. (1984) *Science 24*, 831–838.
de Meyer, R. (1992) Ph.D. Thesis, University of Marburg, Germany.
El Kabbani, O. A. L., Waygood, E. B., & Delbaere, L. T. J. (1987) *J. Biol. Chem. 262*, 12926–12929.
Erni, B. (1989) *FEMS Microbiol. Rev. 63*, 13–24.
Erni, B. (1992) *Int. Rev. Cytol. 137A*, 127–148.
Erni, B., Zanolari, B., & Kocher, H. P. (1987) *J. Biol. Chem. 262*, 5238–5247.
Erni, B., Zanolari, B., Graff, P., & Kocher, H. P. (1989) *J. Biol. Chem. 264*, 18733–18741.
Fairbrother, W. J., Cavanagh, J., Dyson, H. J., Palmer, A. G., Sutrina, S. L., Reizer, J., Saier, M. H., & Wright, P. E. (1991a) *Biochemistry 30*, 6896–6907.
Fairbrother, W. J., Gippert, G. P., Reizer, J., Saier, M. H., & Wright, P. E. (1991b) *FEBS Lett. 296*, 148–152.
Fairbrother, W. J., Palmer, A. G., Rance, M., Reizer, J., Saier, M. H., & Wright, P. E. (1992) *Biochemistry 31*, 4413–4425.
Farmer, B. T., II, Venters, R. A., Spicer, L. D., Wittekind, M. G., & Müller, L. (1992) *J. Biomol. NMR 2*, 195–202.
Fürste, J. P., Pansegrau, W., Frank, R., Blöcker, H., Scholz, P., Bagdasarian, M., & Lanka, E. (1986) *Gene 48*, 119–131.
Génovésio-Taverne, J. C., Sauder, U., Pauptit, R. A., Jansonius, J. N., & Erni, B. (1990) *J. Mol. Biol. 216*, 515–517.
Grdadolnik, S. G., Eberstadt, M., Gemmecker, G., Kessler, H., Buhr, A., & Erni, B. (1994) *Eur. J. Biochem.* (in press).
Grzesiek, S., & Bax, A. (1992a) *J. Magn. Reson. 96*, 432–440.
Grzesiek, S., & Bax, A. (1992b) *J. Am. Chem. Soc. 114*, 6291–6293.
Hammen, P. K., Waygood, E. B., & Klevit, R. E. (1991) *Biochemistry 30*, 11842–11850.
Herzberg, O. (1992) *J. Biol. Chem. 267*, 24819–24823.
Herzberg, O., Reddy, P., Sutrina, S., Saier, M. H., Reizer, J., & Kapadia, G. (1992) *Proc. Natl. Acad. Sci. U.S.A. 89*, 2499–2503.
Ikura, I., Kay, L. E., Bax, A. (1991) *J. Biomol. NMR 1*, 299–304.
Jia, Z., Vandonselaar, M., Quail, J. W., & Delbaere, L. T. J. (1993a) *Nature 361*, 94–97.
Jia, Z., Quail, J. W., Waygood, E. B., & Delbaere, L. T. J. (1993b) *J. Biol. Chem. 268*, 22490–22501.
Kalbitzer, H. R., & Hengstenberg, W. (1993) *Eur. J. Biochem. 216*, 205–214.
Kay, L. E., Clore, G. M., Bax, A., & Gronenborn, A. M. (1990a) *Science 249*, 411–414.
Kay, L. E., Ikura, M., Tschudin, R., & Bax, A. (1990b) *J. Magn. Reson. 89*, 496–514.
Klevit, R. E., & Waygood, E. B. (1986) *Biochemistry 25*, 7774–7781.
Kroon, G. J. A., Grotzinger, J., Dijkstra, K., Scheek, R. M., & Robillard, G.T. (1993) *Protein Sci. 2*, 1331–1341.
Kruse, R., Hengstenberg, W., Beneicke, W., & Kalbitzer, H. R. (1993) *Protein Eng. 6*, 417–423.
Kundig, W., & Roseman, S. (1971) *J. Biol. Chem. 246*, 1407–1418.
Lammers, L. A., Dijkstra, B. W., van Weeghel, R. P., Pas, H. H., & Robillard, G. T. (1992) *J. Mol. Biol. 228*, 310–312.
Liao, D. I., Kapadia, G., Reddy, P., Saier, M. H., Reizer, J., & Herzberg, O. (1991) *Biochemistry 30*, 9583–9594.
Marion, D., Ikura, M., & Bax, A. (1989) *J. Magn. Reson. 84*, 425–430.
Markovic-Housley, Z., Balbach, J., Stolz, B., & Génovésio-Taverne, J. C. (1994) *FEBS Lett.* (in press).
Martin-Verstraete, I., Débarbouillé, M., Klier, A., & Rapoport, G. (1990) *J. Mol. Bol. 214*, 657–671.
Meadow, N. D., Fox, D. K., & Roseman, S. (1990) *Annu. Rev. Biochem. 59*, 497–542.
Messerle, B. A., Wider, G., Otting, G., Weber, C. E., & Wüthrich, K. (1989) *J. Magn. Reson. 85*, 608–613.
Mulligan, M. E., Hawley, D. K., Entriken, R., & McClure, W. R. (1984) *Nucleic Acids Res. 12*, 789–800.
Pelton, J. G., Torchia, D. A., Meadow, N. D., Wong, C. Y., & Roseman, S. (1991a) *Proc. Natl. Acad. Sci. U.S.A. 88*, 3479–3483.
Pelton, J. G., Torchia, D. A., Meadow, N. D., Wong, C.-Y., & Roseman, S. (1991b) *Biochemistry 30*, 10043–10057.
Pelton, J. G., Torchia, D. A., Meadow, N. D., & Roseman, S. (1992) *Biochemistry 31*, 5215–5224.
Pelton, J. G., Torchia, D. A., Meadow, N. D., & Roseman, S. (1993) *Protein Sci. 2*, 543–558.
Postma, P. W., Jacobson, G. R., & Lengeler, J. W. (1993) *Microbiol. Rev. 57*, 543–594.
Powers, R., Gronenborn, A. M., Clore, G. M., & Bax, A. (1991) *J. Magn. Reson. 94*, 209–213.
Presper, K. A., Wong, C. Y., Liu, L., Meadow, N. D., & Roseman, S. (1989) *Proc. Natl. Acad. Sci. U.S.A. 86*, 4052–4055.
Reizer, J., Sutrina, S. L., Wu, L. F., Deutscher, J., Reddy, P., & Saier, M. H. (1992) *J. Biol. Chem. 267*, 9158–9169.
Schmieder, P., Zimmer, S., & Kessler, H. (1991) *Magn. Reson. Chem. 29*, 375–380.
Seip, S., Balbach, J., & Kessler, H. (1992a) *J. Magn. Reson. 100*, 406–410.
Seip, S., Balbach, J., & Kessler, H. (1992b) *Angew. Chem. Int. Ed. Engl. 31*, 1609–1611.
Seip, S., Balbach, J., & Kessler, H. (1993) *J. Biomol. NMR 3*, 233–237.
Sharma, S., Hammen, P. K., Anderson, J. W., Leung, A., Georges, F., Hengstenberg, W., Klevit, R. E., & Waygood, E. B. (1993) *J. Biol. Chem. 268*, 17695–17704.
Spera, S., & Bax, A. (1991) *J. Am. Chem. Soc. 113*, 5490–5492.
Stolz, B., Huber, M., Markovic-Housley, Z., & Erni, B. (1993) *J. Biol. Chem. 268*, 27094–27099.
van Dijk, A. A., de Lange, L. C. M., Bachovchin, W. W., & Robillard, G. T. (1990) *Biochemistry 29*, 8164–8171.
van Dijk, A. A., Scheek, R. M., Dijkstra, K., Wolters, G. K., & Robillard, G. T. (1992) *Biochemistry 31*, 9063–9072.
van Nuland, N. A. J., van Dijk, A. A., Dijkstra, K., van Hoesel, F. H. J., Scheck, R. D., & Robillard, G. T. (1992) *Eur. J. Biochem. 203*, 483–491.
Vuister, G. W., & Bax, A. (1992) *J. Magn. Reson. 98*, 428–435.
Wittekind, M., Rajagopal, P., Branchini, B. R., Reizer, J., Saier, M. H., & Klevit, R. E. (1992) *Protein Sci. 1*, 1363–1376.
Wöhrl, B. M., & Lengeler, J. W. (1990) *Mol. Microbiol. 4*, 1557–1565.
Worthylake, D., Meadow, N. D., Roseman, S., Liao, D. I., Herzberg, O., & Remington, S. J. (1991) *Proc. Natl. Acad. Sci. U.S.A. 88*, 10382–10386.